Field operating window of nanodevices employing the domain wall propagation through the stripes intersection: Numerical optimization

Elena Semenova, Dmitry Berkov, Natalia Gorn, and Roland Mattheis

Citation: Journal of Applied Physics **124**, 153901 (2018); doi: 10.1063/1.5041078
View online: https://doi.org/10.1063/1.5041078
View Table of Contents: http://aip.scitation.org/toc/jap/124/15
Published by the American Institute of Physics

Field operating window of nanodevices employing the domain wall propagation through the stripes intersection: Numerical optimization

Elena Semenova,[1] Dmitry Berkov,[1] Natalia Gorn,[1] and Roland Mattheis[2]
[1]*General Numerics Research Lab, Moritz-von-Rohr-Straße 1A, D-07745 Jena, Germany*
[2]*Leibniz-Institut für Photonische Technologien e.V., Jena, Germany*

(Received 23 May 2018; accepted 15 September 2018; published online 16 October 2018)

In this paper, we present the detailed numerical study of domain wall (DW) dynamics in thin magnetic stripes and in nanostructures containing intersections of such stripes. We focus on the DW propagation through these intersections (crosses), because these are the key elements in field-based multiturn sensors and magnetic logic devices. The DW propagation through such intersections is the main problem by ensuring the functional reliability of the abovementioned devices due to (i) the strong pinning of a DW at these crosses and (ii) the risk that a wrong cross "shoulder" is reversed by the DW propagation. By means of micromagnetic simulations, the operating field range for the desired DW propagation in devices with a constant stripe width is determined, and the drawbacks of this simple design are discussed. To overcome these drawbacks, we suggest a new design employing the stripes with a modulated width. We show that sensors with this design are expected to have a higher reliability and that their field operating window can be controlled in a more flexible way. *Published by AIP Publishing.* https://doi.org/10.1063/1.5041078

I. INTRODUCTION

Domain walls in thin magnetic nanowires (nanostripes) have been under an active investigation for almost 70 years (see, e.g., Chaps. 4 and 6 in Ref. 1 and references therein). These nanostripes are employed in numerous technological applications, like memory devices,[2,3] ultrafast information storage,[4,5] magnetic logic devices,[6] and sensors.[7–10] Dynamics of domain walls in nanostripes with various geometries have been extensively studied both numerically[4,5,9,11–14] and experimentally,[2,15–19] whereby most experimental studies were also accompanied by micromagnetic simulations.

The main subject of this paper is numerical optimization of a DW propagation through the intersection of nanostripes encountered in the layout of magnetic sensors and magnetic logic devices.

Sensors for the detection of a number of revolutions or a linear position play a significant role in modern engineering. DW-based sensors for determining the number of up to 16 turns have been on the market for more than 10 years.[20] These sensors employ the generation of magnetic domains upon rotation of a permanent magnet which generates a field of an appropriate strength. In this case, a 180°-domain wall is generated at each 180° rotation of the magnet and moved into or out of a spiral structure. Due to the geometry of this sensor solution, its detectable field angle range is limited by the number of spiral turns. Therefore, additional technical means are necessary to limit the field rotation within the range of the today's available sensor[20] ranging from 0 to 16 turns. An increase of the number of spiral turns within this concept seems to be possible but is limited to ≈64 turns.

The transition from an open spiral to a combination of closed loops, where every loop is able to count a number of turns prime to the numbers of other loops gives the way for overcoming the limitations described above. As shown in Refs. 10 and 14, a sensor with four loops able to count 5, 7, 11, and 13 turns allows for counting from 0 to 5005 turns. Eight loops (5, 7, 9, 11, 13, 17, 19, and 23 turns) increase the range to $\sim 3.3 \times 10^8$ turns.

The building of closed loops can be done in different ways. A version of closed single loops using cusps is described in Ref. 10. The cusp was proposed as an element acting as a NOT-gate in a DW-based magnetic logic[6] and can be used in a closed loop for extending the counting range by 180° per cusp. By varying the number of cusps from loop to loop, the demand for prime counting of every loop can be easily achieved. Unfortunately, the cusp geometry causes a limitation of the magnetic field range for the safe functionality in a way which is unacceptable for real application.

The second solution employs one of the key entities of modern magnetic devices using the DW movement, namely an intersection of magnetic stripes, realized technologically in a 2D geometry. This holds for turn sensors with a high storage capability (multiturn counter),[14] being capable of counting 10^4–10^8 turns and for the concept of a magnetic logic.[6] The experimental analysis of the domain wall interaction with the cross[21] shows the drawbacks of this element. It limits the field range for a safe domain wall movement.

To overcome this limit, a specially designed syphon-shaped element was proposed[22] and analyzed in Ref. 14 in addition to the cross-shaped intersections of nanowires as displayed in Fig. 1. To avoid pinning of domain walls along the straight nanostripe sections, a minimum field component $H_{\min}$ parallel to these sections is necessary for a secured movement. Additionally, the total field H_{rot} must be below the magnetic field sufficient for the magnetization reversal in the stripe itself (nucleation field H_{nuk}). These values define the field-angle range (as displayed by the gray area in polar plots) for the travel of a domain wall across the intersection for the DW movement from the upper right to the upper left

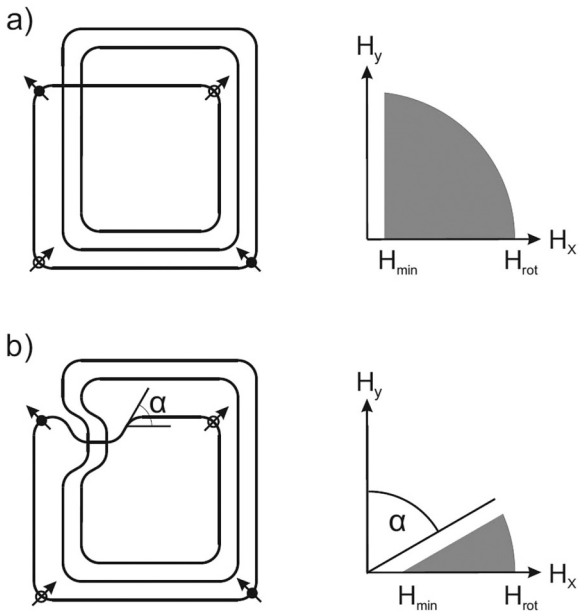

FIG. 1. Closed nanowire loops: (a) with standard stripe intersections and (b) extended by the syphon structure with the angle $\alpha = 60°$; both structures contain two domain walls before (full circles with arrows) and after (open circles with arrows) the magnetic field rotation. Polar plots of the magnetic field range applicable for this movement are shown on the right.

corner and from the lower right to the lower left corner with no intersections as shown in Fig. 1. By adding a syphon shaped element, the field-angle range is remarkably reduced as indicated in the polar plot in Fig. 1(b). As a result, this syphon should prevent counting failures in the sensor structure.

The usage of closed loops with stripe intersections requires a sufficiently broad magnetic field range, where a safe DW transport is guaranteed. Here, the intersection itself forms the limiting element.

Interaction of a DW with a stripe intersection was studied in several publications.[2,14,16,19]

Lewis *et al.*[2,16] have investigated the propagation of a DW in comb structures at relatively low external fields (up to ≈100 Oe) and for stripes having the width of 90 and 100 nm. For these reasons, DW studied in these publications were most probably the so-called transverse walls, and the motion of these walls was mostly laminar. For sensor and logic gate applications, wider stripes (with $w > 200$ nm) and higher applied fields (preferably $H > 200$ Oe) are required, so that additional simulations and experiments covering the corresponding parameter range are necessary. The work of Sethi *et al.*[19] was devoted to DW motion driven by the spin-transfer-torque and the interaction of these walls with stripe intersections in multilayers with strong out-of-plane anisotropy; in our work, we analyze the behavior of sensors based on the GMR effect in multilayered stacks with the *in-plane* magnetization orientation, so that results of Ref. 19 are not applicable to our systems.

In general, various magnetization reversal scenarios can occur by the DW motion through these intersections. Among them, the scenario which ensures the proper sensor functioning should obey the following conditions: (i) the DW should pass through the intersection without being pinned, (ii) the DW may not cause the reversal of the "wrong" intersection branch, and (iii) the reversal of the "correct" branch should occur due to the DW motion—when it reaches the intersection, rather than start (nucleate) at the intersection itself. The minimal and maximal fields $H_{\min}$ and $H_{\max}$, for which all these conditions are fulfilled, determine the lower and upper bounds of the so-called field operating window (FOW).

DW pinning is observed if the applied field is too weak, so that the strong magnetodipolar field induced by the intersection edges does not allow the DW to pass. Obviously, the minimal field required to overcome this pinning represents the lower FOW boundary $H_{\min}$.

Magnetization reversal of the undesired cross shoulder can occur either if the angle of the applied field is not chosen properly or if the field magnitude is too large. The first problem may be avoided by the insertion of the "syphon" structures as explained above. However, even for the proper field angle, the cross shoulder without the DW can also be reversed if the field magnitude exceeds some critical value, denoted below as $H_{\mathrm{cr}}^{(1)}$. Such a reversal of both intersection shoulders clearly would lead to the failure of the sensor.

Finally, for fields above a certain threshold, magnetization reversal of the "correct" shoulder may occur not due to the DW motion along this shoulder, but due to the nucleation reversal at the cross itself. We denote the corresponding critical field as $H_{\mathrm{cr}}^{(2)}$. This kind of reversal is possible, because the effective structure width at the intersection of two stripes is larger than that of a single stripe. Hence, the shape anisotropy at the intersection is smaller than the anisotropy of the stripe itself. For this reason, the cross represents a potential nucleation site. This kind of reversal should be avoided, because the functional principle of any sensor or logic device heavily relies on the assumption that the reversal occurs solely due to the motion of the injected DW along the corresponding stripe.

Thus, the upper FOW boundary $H_{\max}$ is given by the smallest of the two critical fields $H_{\mathrm{cr}}^{(1)}$ and $H_{\mathrm{cr}}^{(2)}$ defined above. We note already here that both these fields depend on the field orientation.

In this paper, our primary goal is to determine and to optimize the FOW for nanodevices containing intersections of magnetic stripes. For this purpose, we first develop a methodology to determine the field range for which the DW passage through these intersections obeys the three conditions outlined above. Afterwards, we perform the comparative analysis of various intersection layouts in order to determine which of them provides the optimal conditions for the reliable DW propagation.

II. MICROMAGNETIC SIMULATIONS: METHODOLOGY OF THE QUASISTATIC AND DYNAMIC MODELLING

All micromagnetic simulations of quasistatic and dynamic switching processes were performed using our software package MicroMagus[23] adapted to the graphic processing units (GPU).

We consider thin film structures made of $Ni_{81}Fe_{19}$ (Py) with the saturation magnetization $M_s = 800$ G, exchange

constant $A = 1 \times 10^{-6}$ erg/cm, negligibly small magnetocrystalline anisotropy, and Gilbert damping $\lambda = 0.01$; the latter quantity is used in dynamical simulations only. Modelling of systems made of other materials (e.g., CoFe alloys) has produced qualitatively similar results and is not discussed in this paper.

Both for quasistatic and dynamic simulations, we consider the cross made of stripes with the thickness $h = 32$ nm and either the constant width $w = 250$ nm (Sec. III A) or the sine-modulated width (Sec. III B). The discretization cell size is $5 \times 5 \times 8\,\text{nm}^3$; it was checked that further discretization refinement did not lead to noticeable changes in results. We note that although the stripe thickness h is relatively small, it is still several times larger than the characteristic micromagnetic length for Py ($l_{\text{dem}} \sim \sqrt{A/M_s^2} \approx 10$ nm). Hence, discretization of the stripe into several in-plane layers is necessary. Corresponding test runs have shown that if this discretization is absent or insufficient, magnetization dynamics cannot be captured correctly. In particular, the transition from the laminar to turbulent motion occurs at higher fields. Further, typical magnetization structures arising by the turbulent motion are different from those observed in stripes with the sufficiently fine discretization in the out-of-plane direction.

The lateral size of the simulated area is $4 \times 4\,\mu\text{m}^2$ for quasistatic and $6 \times 2\,\mu\text{m}^2$—for dynamic simulations. The "smoothing" of inner intersection corners, unavoidably arising by manufacturing, is taken into account by rounding these corners with the radius $R_c = 100$ nm.

We note already here that increasing the stripe width in technologically relevant region, between 250 and 350 nm, leads to the FOW shift toward smaller field values but does not lead to qualitative changes of simulation results.

For quasistatic simulations, the initial magnetization state of the cross along with the coordinate system and geometrical parameters are depicted in Fig. 2. Periodic in-plane boundary conditions (BC) were used to avoid the switching nucleation at the stripe edges adjacent to the boundary of the simulation area. For open BC, such a nucleation can take place at these edges due to the strong demagnetizing field.

We use these simulations to quickly estimate the upper FOW boundary by determining the switching field of the configuration shown in Fig. 2. This field is obtained in the following way. We first calculate the equilibrium magnetization state at zero external field. Then, we increase the magnitude of this field by a small step of typically $\Delta H = 2 - 5$ Oe, applying the field at a certain angle α to the horizontal axis and determining again the equilibrium state. When the magnetization of at least one cross shoulder reverses (switches), we define this field as the switching field for this angle α and for this shoulder. To obtain the whole dependence $H_{\text{sw}}^{\text{qs}}(\alpha)$ (see Figs. 3 and 9), the field direction α is varied from 5° to 85°.

Simulations of this kind give us the upper FOW boundary in dependence on the field direction without extremely time-consuming dynamic simulations.

Dynamic micromagnetic simulations are performed according to the following protocol.

First, a counter-clockwise vortex DW is generated on the left end of the horizontal stripe and the equilibrium magnetization state without the external field is obtained. This choice of the initial state can be justified as follows. In principle, as shown in Ref. 18, DW propagation along the stripe and especially its behavior at the stripe fork can strongly depend on the initial DW state (e.g., rotation sense for a vortex wall). However, this dependence exists only if the DW motion is laminar, so that well-defined vortices and half-vortices are formed during its motion, as it was the case for relatively low

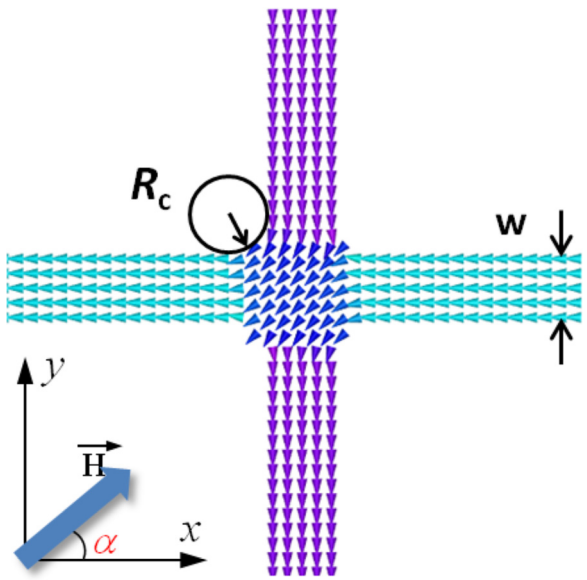

FIG. 2. Initial magnetization and geometry parameters of the simple cross.

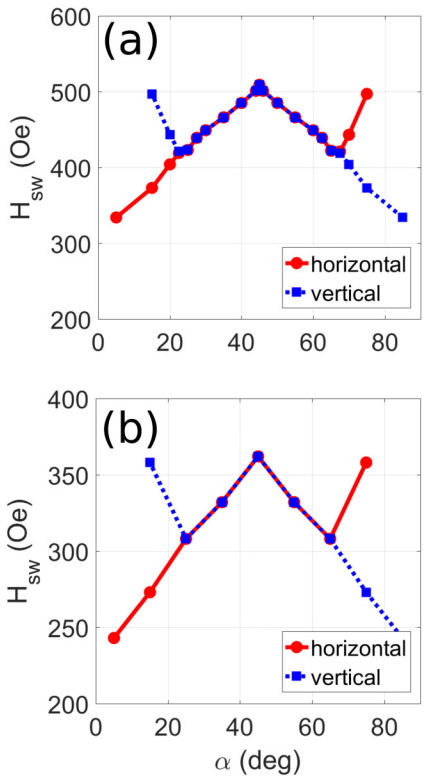

FIG. 3. Dependence of the quasistatic switching field on the field direction for the cross of stripes having the width $w = 250$ nm (a) and $w = 350$ nm (b). Red curves correspond to the switching of the horizontal stripe, the blue ones—of the vertical stripe.

spin-polarized current values used in Ref. 18. For our stripes, in the external field region corresponding to FOW, the DW motion is always turbulent. For this motion type, the "memory" about the initial DW state is quickly lost, so that the initial DW configuration is not important. We also note that the same (vortex) DW was used as the initial magnetization state in Ref. 14, where a similar problem was studied.

Next, the external field with a prescribed magnitude and direction is applied, causing the DW movement. Corresponding magnetization dynamics is monitored either till one or both stripe(s) of the structure are completely reversed, or until the DW is pinned at the intersection.

Periodic BC were applied also for this kind of simulation. In order to avoid the incompatibility of these BC with the motion of a single domain wall, the horizontal cross shoulder was cut several discretization cells away from the simulation area boundary. It was checked that the magnetodipolar field from the artificial free edges arising because of this cut did not influence DW propagation through the stripe intersection (which was at least 4 μm away from these borders).

Such dynamic simulations allow one to determine, first, the *lower* FOW boundary $H_{\min}(\alpha)$, defined as the minimal field that allows the DW to pass the stripe intersection without being pinned. Second, these simulations allow a more precise determination of the *upper* FOW boundary $H_{\max}$: This field, obtained by dynamic simulation, may be less than the "quasistatic" upper FOW boundary H_{sw} discussed above, due to various dynamical effects as, e.g., strong inhomogeneities of magnetic configurations caused by the dynamic reversal nucleation.

In our simulations, we do not take into account thermal fluctuations ($T = 0$). These fluctuations would slightly decrease the lower FOW boundary, because thermal activation would allow a DW to overcome the pinning energy barrier with a finite probability for $H < H_{\min}(T = 0)$. For the same reason, the upper FOW boundary (i.e., both $H_{cr}^{(1)}$ and $H_{cr}^{(2)}$) would also become somewhat smaller. However, taking into account a relatively large width and thickness of the stripes considered here, we do not expect this effect to be significant. Further, thermal fluctuations would make the DW motion even more turbulent than it already is without these fluctuations (see the corresponding discussion in Sec. III). The quantitative analysis of the corresponding effect requires a large number of simulations for identical model parameters, but with different realization of thermal fluctuations, which is beyond the modern computer capabilities for systems as large as studied here. In any case, the system behavior in the absence of thermal fluctuations should be understood first, which is the main goal of this paper.

III. RESULTS AND DISCUSSION

A. Intersection of stripes having a constant width

1. Quasistatic switching field

We start with the analysis of the quasistatic switching behavior of the intersection of stripes having the constant width (the "simple" cross). Switching field dependencies on the field angle for the magnetization reversal of the horizontal and vertical stripes, starting from the initial state shown in Fig. 2, are presented in Fig. 3 with the red and blue lines correspondingly.

For the stripe width $w = 250$ nm [Fig. 3(a)], the horizontal stripe switches first at the external field angles $\alpha < 23°$, because for these angles, the field projection on the horizontal direction is much larger than on the vertical one. An example of the magnetization states just before ($H = 403$ Oe) and immediately after ($H = 405$ Oe) the switching of the horizontal stripe for $\alpha = 20°$ is given in Fig. 4. It can be clearly seen that the switching nucleates at the stripes intersection are as explained above.

Due to the symmetry of the system with respect to the angle $\alpha = 45°$, the switching process for $\alpha > 67°$ follows the opposite scenario, namely, the vertical stripe reverses first and the horizontal one in a larger field.

The most interesting feature of these $H_{sw}(\alpha)$-dependencies is the simultaneous switching of both stripes for angles between $23° < \alpha < 67°$. Such simultaneous switching means an additional dynamic instability in the sense that more parts of the sensor layout can be affected by the switching in the above-mentioned angle range. In other words, in this angle range, we cannot enforce the (quasistatic) magnetization reversal of only one cross "shoulder."

The origin of this behavior, as demonstrated in Fig. 4, is the peculiarity already discussed above: the reversal process starts at the cross intersection, because it is the widest part of the system. Since the intersection is situated at both the horizontal and the vertical stripes, the nucleation of the magnetization reversal in this region may cause the simultaneous reversal of both stripes, which indeed happens in the wide angle range.

The cross of stripes having a larger width $w = 350$ nm has a qualitatively similar switching field dependence on the field angle [Fig. 3(b)]. The magnitude of the switching field is smaller than for $w = 250$ nm due to the smaller nucleation field for a stripe with larger width and the same thickness. The relation of the switching fields for these two cases is approximately equal to the relation of the stripe widths.

As explained above, this way the "quasistatic" upper FOW boundary for such sensors as the function of the field angle $H_{\max}(\alpha)$ can be determined. The operating fields allowed for the reliable functioning of magnetic nanodevices based on a layout with intersections should be well below the smallest switching field for all possible field angles.

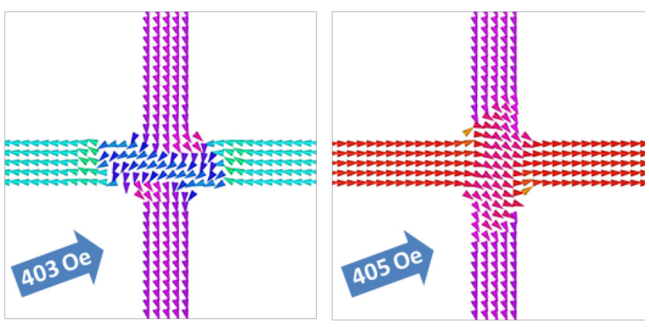

FIG. 4. Equilibrium magnetic configuration of the cross just before ($H = 403$ Oe) and immediately after ($H = 405$ Oe) switching at the field direction $\alpha = 20°$.

2. Dynamics of the DW passage through the simple cross

All results presented below are obtained for the field direction $\alpha = 20°$, which, according to quasistatic simulations, lies outside the range where both stripes reverse simultaneously. This angle was chosen for technological reasons because it is a convenient angle for a common sensor design including the syphon element.[14]

We begin with the determination of the lower FOW boundary, which should exceed the pinning field. Starting, as explained in Sec. II, from the vortex DW at the left end of the horizontal cross shoulder [Fig. 5(a)], for small fields we arrive at a typical "pinned" DW configuration shown in Fig. 5(b): the wall stops at the intersection and cannot pass the cross. The lower critical field at which the DW passes the cross is determined by a successive increase of the applied field magnitude in steps of $\Delta H = 10$ Oe; for this angle, we obtain $H_{\min}(\alpha = 20°) = 115(\pm 5)$ Oe.

Further increase of the applied field—up to ≈375 Oe—allows the DW to pass the intersection, reversing the horizontal stripe because of the motion of this DW and without causing the reversal of the vertical stripe. Hence, in the field interval $115 \leq H \leq 375$ Oe, we find the desired DW propagation pattern for this type of sensors, as discussed in the Introduction. The corresponding example is shown in Fig. 6 for $H = 300$ Oe.

However, already for the fields within this range which are much weaker than the maximal operating field, the DW motion is strongly turbulent. Even in the absence of thermal fluctuations, this kind of motion results in very different realizations of remagnetization processes by very small changes of initial conditions, like the starting position of DW. Such a behavior could lead to an instability of a multiturn sensor, if for some especially unfortunate realization of the turbulent motion, the DW passage would result also in the reversal of the vertical cross shoulder. This problem will be addressed below.

For fields above this critical field $H > H_{cr}^{(2)} \approx 375$ Oe (but still well below the "quasistatic" switching field), we observe the 2nd type of the undesired behavior mentioned above. The reversal of the horizontal stripe starts at the intersection, instead of being induced by the DW motion. A snapshot of the corresponding magnetization configuration is shown in Fig. 7(a). This behavior is unwanted because the functioning of this multiturn sensor relies on the assumption that magnetization reversal occurs due to the DW motion. We point out that this upper "dynamic" critical field is smaller than the corresponding "quasistatic" switching field ($H_{sw} \approx 404$ Oe). Therefore, the FOW is additionally reduced when compared to the "quasistatic" upper FOW boundary, which should be taken into account when optimizing the sensor design.

By further increasing the field, both stripes are reversed exhibiting the 3rd type of the undesired magnetization switching. An example of such a behavior is shown in Fig. 7(b), where the final magnetization configuration for $H = 440$ Oe is displayed. This dynamic critical field $H_{cr}^{(1)}$ coincides, within the field step used in our study, with the "quasistatic" switching field H_{sw} for the vertical cross shoulder (see the blue line in Fig. 3). However, this process is irrelevant for the sensor optimization, because for this stripe

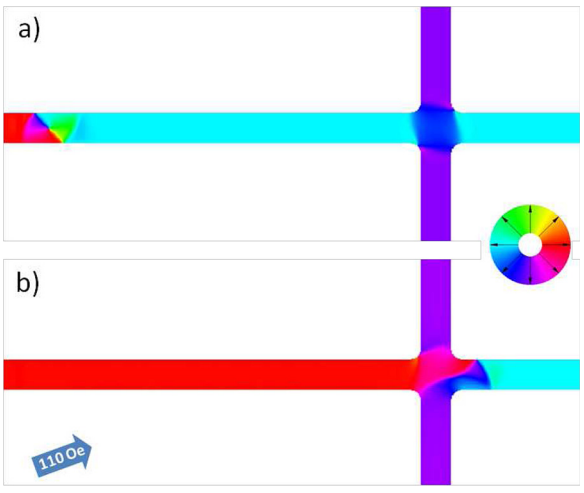

FIG. 5. (a) Equilibrium state with the vortex DW ($H = 0$); (b) DW pinning at $H = 110$ Oe.

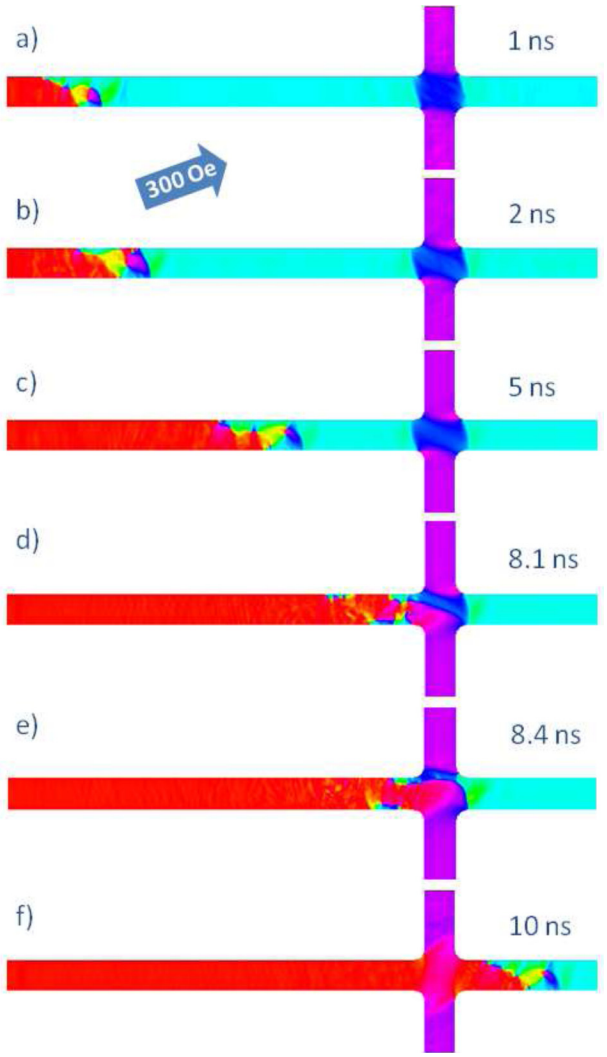

FIG. 6. Snapshots of the DW motion at different time moments by passing the cross intersection at $H = 300$ Oe.

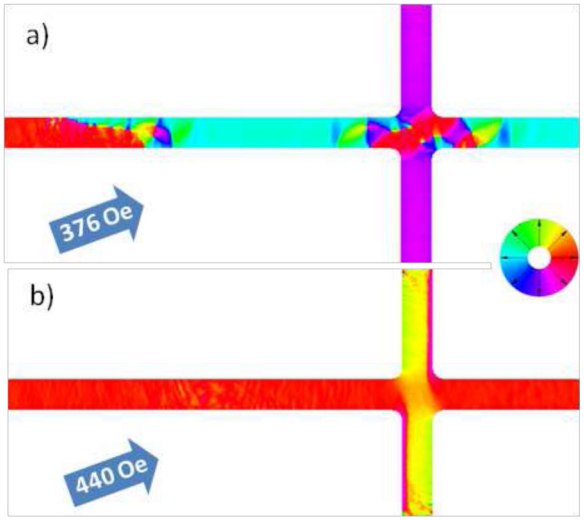

FIG. 7. Undesired reversal behavior (a) of the 2nd kind at $H = 376$ Oe: remagnetization starts at the stripe intersection and (b) of the 3rd kind at $H = 440$ Oe: magnetization of both stripes reverses.

geometry and material parameters, the undesired reversal of the 2nd kind already takes place at lower fields. Hence, the upper boundary of FOW determined from dynamic simulations is equal to the second critical field $H_{cr}^{(2)}(\alpha = 20°) = 375 \pm 2$ Oe.

Based on these results, we conclude that the cross consisting of two stripes with the constant width has the following drawbacks: (1) DW motion is highly complicated (turbulent), which could lead to sensor failure for some unfortunate realization of this turbulent motion; (2) the sensitivity of the upper working field to the field direction $\partial H/\partial\alpha$ in the angle range $0 < \alpha < 45°$ is approximately constant and relatively high: $\partial H/\partial\alpha \approx 4$ Oe/deg as shown in Fig. 3; (3) in a wide angle region ($23° < \alpha < 67°$ for $w = 250$ nm), the horizontal and vertical stripes switch at the same field, introducing an additional ambiguity to the quasistatic switching process of the system under study. Although, as explained above, this kind of instability is not important for the dynamical reversal caused by a DW for system parameters used in our simulations, it might play an important role in other applications.

B. Intersection of stripes having a modulated width

To overcome the problems of the constant-width design, we propose to use stripes with a modulated width. In particular, we analyze the behavior of a DW in stripes having a sine-modulated width

$$w(x) = w_0 - A\cos\left(\frac{2\pi x}{\Lambda}\right), \tag{1}$$

where parameters A and Λ represent correspondingly the amplitude and the wavelength of the modulation. As it is well known, the DW motion in stripes with smaller width is generally more laminar (for the same external field). Hence, the basic idea behind the usage of modulated-width stripes is to reduce the turbulence of the DW motion.

We have varied the modulation amplitude and wavelength in the technologically reasonable range $A = 10-30$ nm and $\Lambda = 500-1000$ nm. Below, we present exemplary results for the stripe with $w_0 = 250$ nm, $A = 30$ nm, and $\Lambda = 1000$ nm. Results for other parameter values are qualitatively similar.

The advantage of this stripe geometry can be seen already by dynamic simulations of a single stripe. In Fig. 8, we present magnetization configuration snapshots for the constant-width and modulated-width stripes, whereby the maximal stripe width for the second case is equal to the constant stripe width for the first case. These snapshots demonstrate a significant decrease of the DW motion turbulence in narrow regions of the modulated stripe. Whereas in the broad part of this stripe we still observe a complex turbulent DW motion [Figs. 8(a) and 8(c)], in narrow parts the single vortex structure is recovered [Figs. 8(b) and 8(d)], making the wall motion more deterministic. Further, this motion remains almost deterministic also within a short distance after this point. Such a behavior should increase the probability that a DW passes the stripes' intersection in a well-controlled manner, when this intersection is placed at or immediately after the narrow region of the width-modulated stripe.

Here, it should be mentioned that DW propagation in stripes with a non-constant width has been studied in several papers.[5,11–13] Nakatani *et al.*[5] and Albert *et al.*[13] have simulated nanowires with a *randomly* fluctuating width (edge roughness). In Ref. 5, the influence of roughness on the DW dynamics in nanostripes with the small thickness approximately equal to the characteristic micromagnetic length of Py ($h = 5$ nm), and in relatively low fields (up to 60 Oe), has been investigated. In Ref. 13, very narrow nanowires ($w = 20$ nm) with the strong perpendicular anisotropy have been studied. For these reasons, results of these two papers cannot be directly compared to our simulations.

Domain wall propagation in stripes with a sine-modulated width was simulated in Refs. 11 and 12. In these papers,

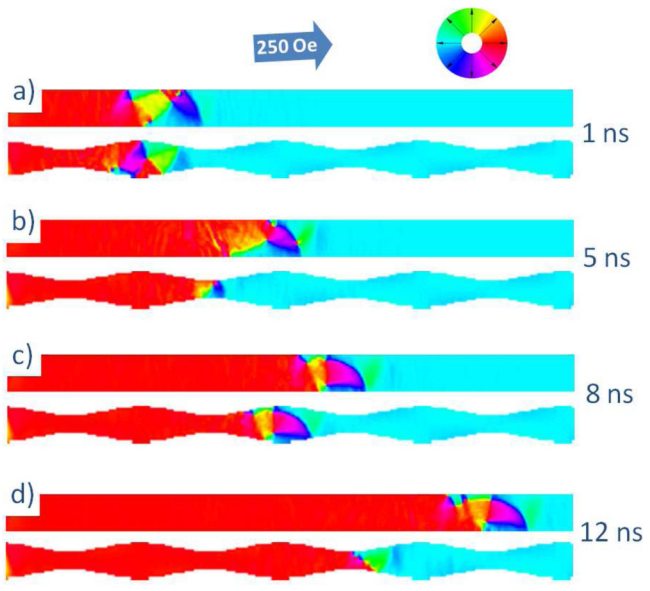

FIG. 8. Features of the DW dynamics in a simple stripe and a width-modulated stripe at $H = 250$ Oe at different time moments.

much thinner ($h = 10$ nm) and narrower ($w = 100$ nm) stripes have been investigated, by simulating the DW motion in a relatively high applied field $H = 300$ Oe. Due to the smaller cross section of stripes in Refs. 11 and 12, DW patterns shown in these papers are less chaotic than in our simulations. Vortex formation in the narrow parts of the stripe can be recognized in Fig. 2 from Ref. 11, being in accordance with our findings.

We note here that the possibility to control the DW motion in nanowires using their edge roughness or deterministically modulated width was suggested for the first time in Ref. 5. In this paper, it was shown that roughness can strongly increase the DW velocity in fields above the Walker breakdown due to the suppression of the antivortex nucleation at rough edges and transition to the turbulent DW motion. In our case, the fields of interest (FOW) are always higher than the Walker breakdown field, and the DW motion is turbulent already in the perfect stripe. For this reason, the DW velocity in our width-modulated stripe is somewhat smaller than in the perfect stripe (see Fig. 8) but still very high: $v \sim$ 200-400 m/s. These large values open up a possibility to optimize magnetic parameters and geometry of our stripes with respect to potential applications in high-frequency sensors.

Next, we present simulation results for the stripe cross, where modulated-width stripes intersect at their narrowest parts. Rounding of the intersection corners with the radius $R_c = 100$ nm is also assumed.

For this design, we have simulated the quasistatic switching process first, performing it in the same way as for the cross of constant-width stripes.

Corresponding dependencies of the switching field H_{sw} on the field direction α are shown in Fig. 9. First of all, for the intersection of width-modulated stripes, there is no angle range where the two stripes reverse simultaneously. To explain this feature, we recall that in a cross made of constant-width stripes, the switching starts in the intersection region itself, due to the largest effective width of the structure in this region, which results in the simultaneous switching of both stripes in the wide angular range. In contrast to this simple system, for modulated-width stripes, magnetization reversal starts in the broadest parts of that stripe, for which

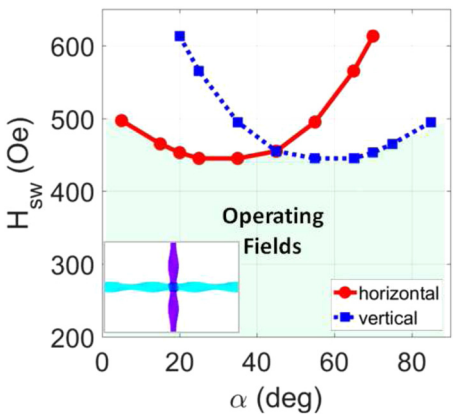

FIG. 9. Quasistatic switching field dependence on the field direction for the "modulated-width" cross.

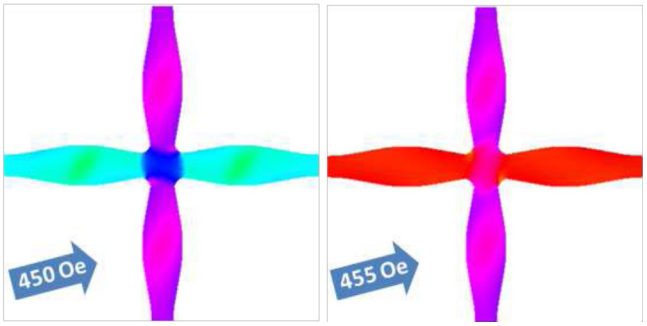

FIG. 10. Equilibrium magnetic configurations just before ($H = 450$ Oe) and immediately after ($H = 455$ Oe) switching for the field angle $\alpha = 20°$.

the field projection on its direction is larger (Fig. 10). The other stripe is therefore not affected by this reversal nucleation. Hence, the two stripes are now completely decoupled, which makes the system more stable, offering more freedom in choosing the field direction and ensuring a higher sensor reliability.

Further, the sensitivity of the switching field magnitude to the field angle is significantly reduced: for the stripe which reverses first, the sensitivity does not exceed $\partial H/\partial\alpha \approx 3$ Oe/deg. We also note that the smallest switching field for this design is about 100 Oe larger than for the constant-width cross. This is due to the circumstance that for the modulated-width cross, the maximal structure width is equal to the maximal stripe width w_0, whereas for the constant-width design, it is approximately $\sqrt{2}w_0$.

The switching mechanism explained above is similar to that described in Ref. 15 (see Fig. 6 in the corresponding paper). However, our switching fields are much larger compared to $H_{sw} \approx 160$ Oe for the stripe thickness $h = 5$ nm and $H_{sw} \approx 250$ Oe for $h = 10$ nm found in Ref. 15 for the stripe with similar modulation parameters. This difference is due to a much larger thickness of our stripes.

We proceed with the analysis of dynamic simulation results of the DW motion through the modulated-width intersection. First, we determine the lower FOW boundary. Due to the smaller width of the stripes at the intersection, the corresponding pinning field is generally higher for the modulated-width system than for a "simple" cross. In particular, for our modulation parameters, the pinning field is $H_{pin} = 240(\pm 5$ Oe), thus being 130 Oe larger than for the "simple" cross (for the same angle $\alpha = 20°$). This feature might be advantageous for devices which should operate in environmental conditions involving undesired interference magnetic fields.

The desired pattern of the DW propagation for our system is observed in the field range $240 < H < 440$ Oe at $\alpha = 20°$. The corresponding example for $H = 250$ Oe is presented in Fig. 11. The comparison of magnetization configurations by the wall propagation through the intersection for the modulated-width system [Figs. 11(d) and 11(e)] and for the cross made of constant-width stripes [Figs. 6(d) and 11(e)] clearly shows that for the former case, DW motion is much less turbulent, which should lead to a better stability of the reversal process. Unfortunately (similar to the

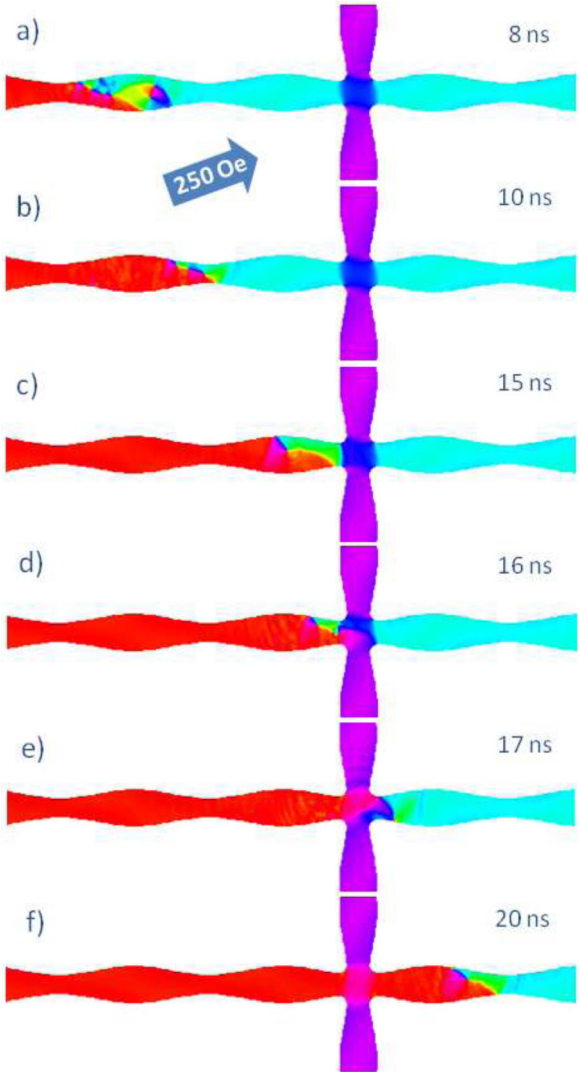

FIG. 11. Snapshots of the DW motion at different time moments by passing the cross intersection at $H = 250$ Oe.

analysis of the thermal fluctuation effect), the quantitative confirmation of this hypothesis requires simulations of a very large number of passage events for both intersection designs under slightly different initial conditions. As mentioned above, such "high-throughput" micromagnetic simulations for the system under study are at present out of range of commonly used computer capabilities.

The upper FOW boundary corresponds also for this design to the failure event of the 2nd type. The reversal of the horizontal stripe starts near the intersection, instead of being induced by the DW motion. The difference to the constant-width case is that in the modulated-width system, this reversal starts at broad parts of the stripes near the intersection, analogously to the quasistatic switching process, and not within the intersection itself [compare Figs. 12(a) and 7(a)]. The reason for this difference is the same as by the quasistatic switching.

We note that for this intersection design, we observe a better agreement between the "quasistatic" switching field ($H_{sw} \approx 452$ Oe) shown in Fig. 9 and the dynamical upper FOW boundary $H_{max} \approx 442$ Oe than for the "simple" cross.

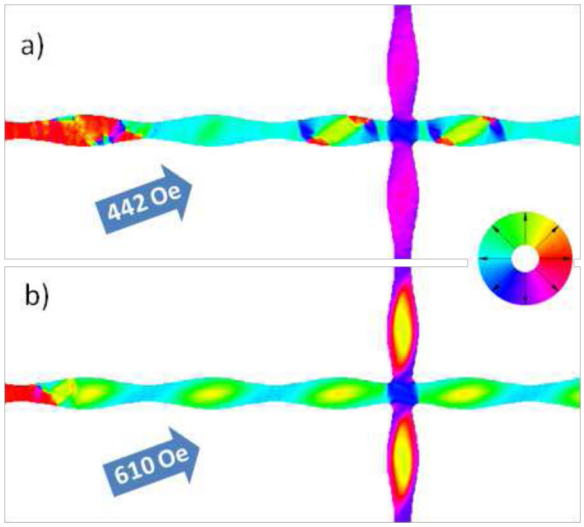

FIG. 12. Undesired reversal behavior (a) of the 2nd kind and (b) of the 3rd kind for the modulated-width intersection.

Hence, for this system, we have a possibility to estimate the upper FOW limit using quasistatic modeling, thus avoiding time-consuming dynamic simulations.

Reversal of both stripes (failure event of the 3rd kind) takes place at fields $H \geq 610$ Oe, whereby the nucleation occurs in broader parts of both stripes [Fig. 12(b)].

From dynamic simulations, it can therefore be concluded that the field operating window for the modulated-width intersection shifts toward higher fields compared to the constant-width cross. As mentioned above, this can be an additional advantage for applications, reducing the influence of all types of interference fields from the environment, thus allowing better control over the magnetization reversal process.

In addition, varying the two geometrical modulation parameters (amplitude and wave length) offers the possibility for a better control of the FOW in such sensors, adjusting this window for any particular application.

The range of width modulation parameters for the sensor optimization is determined by the desired FOW and technological requirements. In particular, the minimal stripe width is dictated by the technical limit with respect to the reliable stack patterning: a too small nominal width can cause the unacceptably high fraction of rejects due to the unavoidable edge roughness. This circumstance poses the upper limit on the modulation amplitude A. On the other hand, too small amplitudes would have only a negligible effect of the intersection FOW. Decrease of the modulation wavelength Λ leads to the increase of the minimal field required to move a DW along the stripe, whereas a wavelength much larger than the stripe width would not eliminate the turbulent motion of a DW in the vicinity of the cross structure. According to our estimation, for Permalloy stripes the parameter range $A = 10$–30 nm and $\Lambda = 500$–1000 nm mentioned above is most suitable for the design optimization of GMR-based sensors.

IV. CONCLUSION

Based on micromagnetic simulation results, we suggest a new design of the stripe intersection for field-based

multiturn sensors and magnetic logic gates. This design should provide a more reliable functioning of these devices and better possibilities to adjust their field operating window. For this purpose, we propose to use stripes with sine-modulated width. The domain wall propagation along such stripes is less turbulent, because in the narrow parts of a stripe, a deterministic single vortex structure of a DW is recovered. Further, the proposed stripe geometry provides higher dynamical stability of the magnetization reversal at a stripe intersection, because the reversal process starts at the broader parts of the corresponding stripe, so that the magnetization of only the desired stripe is reversed for any field direction, when the field magnitude is increased. In addition, the corresponding switching field value is less sensitive to the field direction than for the constant-width design. Finally, the intersection of width-modulated stripes allows one to work in larger fields, making the device less sensitive to external magnetic noise.

ACKNOWLEDGMENTS

We acknowledge the German Federal Ministry for Economic Affairs and Energy for its financial support in frames of the INNO-KOM project MF 150023 "MAGSIMSENS."

[1]T. Shinjo, *Nanomagnetism and Spintronics* (Elsevier, 2015).
[2]E. R. Lewis, D. Petit, L. O'Brien, A. Fernandez-Pacheco, J. Sampaio, A.-V. Jausovec, H. T. Zeng, D. E. Read, and R. P. Cowburn, Nat. Mater. **9**, 980 (2010).
[3]S. S. P. Parkin, M. Hayashi, and L. Thomas, Science **320**, 190 (2008).
[4]J.-Y. Lee, K.-S. Lee, and S.-K. Kim, Appl. Phys. Lett. **91**, 122513 (2007).
[5]Y. Nakatani, A. Thiaville, and J. Miltat, Nat. Mater. **2**, 521 (2003).
[6]A. Allwood, G. Xiong, C. Faulkner, D. Atkinson, D. Petit, and R. P. Cowburn, Science **309**, 1688 (2005).
[7]M. Diegel, R. Mattheis, and E. Halder, IEEE Trans. Magn. **40**, 2655 (2004).
[8]R. Mattheis, M. Diegel, U. Hubner, and E. Halder, IEEE Trans. Magn. **42**, 3297 (2006).
[9]M. Diegel, S. Glathe, R. Mattheis, M. Scherzinger, and E. Halder, IEEE Trans. Magn. **45**, 3792 (2009).
[10]R. Mattheis, S. Glathe, M. Diegel, and U. Hübner, J. Appl. Phys. **111**, 113920 (2012).
[11]H.-G. Piao, J.-H. Shim, S.-H. Lee, D. Djuhana, S.-K. Oh, S.-C. Yu, and D.-H. Kim, IEEE Trans. Magn. **45**, 3926 (2009).
[12]H.-G. Piao, J.-H. Shim, D. Djuhana, S.-H. Lee, S.-H. Jun, C.-M. Heo, S.-K. Oh, S.-C. Yu, and D.-H. Kim, IEEE Trans. Magn. **46**, 224 (2010).
[13]M. Albert, M. Franchin, T. Fischbacher, G. Meier, and H. Fangohr, J. Phys.: Cond. Matt. **24**, 024219 (2012).
[14]B. Borie, M. Voto, L. Lopez-Diaz, H. Grimm, M. Diegel, M. Kläui, and R. Mattheis, Phys. Rev. Appl. **8**, 044004 (2017).
[15]D. Burn, E. Arac, and D. Atkinson, Phys. Rev. B **88**, 104422 (2013).
[16]E. R. Lewis, D. Petit, A.-V. Jausovec, L. O'Brien, D. E. Read, H. T. Zeng, and R. P. Cowburn, Phys. Rev. Lett. **102**, 057209 (2009).
[17]M. Muoz and J. Prieto, Nat. Comm. **2**, 562 (2011).
[18]A. Pushp, T. Phung, C. Rettner, B. Hughes, S.-H. Yang, L. Thomas, and S. Parkin, Nat. Phys. **9**, 505 (2013).
[19]P. Sethi, C. Murapaka, G. Lim, and W. Lew, Appl. Phys. Lett. **107**, 192401 (2015).
[20]Novotechnik, see http://www.novotechnik.com for information on characteristics of available sensor types (2011).
[21]D. Atkinson, C. Faulkner, D. Allwood, and R. Cowburn, in *Spin Dynamics in Confined Magnetic Structures III*, edited by B. Hillebrands and A. Thiaville (Springer-Verlag Berlin Heidelberg, 2006), Chap. 6.
[22]M. Diegel and R. Mattheis, "Magnetic sensor for absolute counting of revolutions or linear distances," German patent DE 102013018680 (5 July 2015).
[23]D. Berkov and N. Gorn, See http://micromagus.de for "Micromagus: Package for micromagnetic simulations."